Hindawi Publishing Corporation
Shock and Vibration
Volume 2016, Article ID 6928686, 13 pages
http://dx.doi.org/10.1155/2016/6928686

Research Article

Study of the Influences of Transient Crack Propagation in a Pinion on Time-Varying Mesh Stiffness

Youmin Hu, Jikai Fan, and Jin Yu

State Key Laboratory of Digital Manufacturing Equipment and Technology, Huazhong University of Science and Technology, Wuhan, Hubei 430074, China

Correspondence should be addressed to Jikai Fan; fan_ji_kai@163.com

Received 21 April 2016; Revised 15 August 2016; Accepted 29 August 2016

Academic Editor: Ivo Caliò

Cracks in a cracked gear may further propagate by a tiny length in a very short time for several reasons, such as material fatigue and load fluctuations. In this paper, this dynamic process is defined as transient propagation of cracks. This research aims to calculate the time-varying mesh stiffness of gears when transient propagation of cracks arises, which has not been extensively studied in existing literatures. The transient propagation of cracks is modelled. An improved potential energy method is proposed by incorporating the propagation model into the potential energy method. The improved method can also be utilised to calculate the mesh stiffness of gears when transient propagation of cracks arises. Different transient propagation models are considered to simulate the propagation of cracks in a short amount of time. Different deterioration levels of cracks before transient propagation and different lengths and models of transient propagation are also examined. The variation rules of mesh stiffness caused by the transient propagation of cracks are summarised. The influence of the deterioration level of cracks on mesh stiffness variation when transient propagation arises is obtained. Simulation results show that the proposed method accurately calculates time-varying mesh stiffness when transient propagation of cracks arises. Furthermore, the method improves the monitoring of further propagation of cracks in gears from the perspective of time-varying mesh stiffness.

1. Introduction

Root crack, a typical fault in gear sets, may result from poor operating conditions, such as inadequate lubrication, excessive applied torque, poor specifications, material defects, and manufacturing or installation problems [1]. Undesirable dynamic responses, including serious vibration and noise, may generate once a crack appears, and this occurrence may shorten the service life of a gear [2, 3]. Therefore, reducing catastrophic accidents by improving the detection of crack faults is highly significant.

Time-varying mesh stiffness, which is caused by the periodic change of working teeth pairs, is an important parameter in the gear system. On the one hand, it brings about inherited periodic internal excitations of the gear system [3]; on the other hand, time-varying mesh stiffness decreases when a gear crack appears [5]. Therefore, both crack propagation and the resultant reduction in time-varying mesh stiffness have elicited the interest of many researchers [6, 7]. The current work also belongs to this research field.

In their research on crack propagation, Lewicki and Ballarini studied the influence of rim thickness on crack propagation path [8], set up different fatigue crack growth models to predict crack propagation life for thin rim teeth [9], and proposed a method to study the influence of tooth dynamic loading on crack propagation [10]. Based on linear elastic fracture mechanics, Pandya and Parey [11] adopted a 2D finite element method to study crack propagation paths in gear pairs with different contact ratios. In their recent studies [3, 12, 13], they studied the influence of backup ratio (rim thickness-to-tooth height), fillet radius, and pressure angle on crack propagation and mesh stiffness in gear pairs with a low contact ratio. The finite element method based on linear elastic fracture mechanics (LEFM) was developed to study the crack propagation path of spur gears with a high contact ratio (HCR) and with tooth root cracks for two gear

parameters (backup ratio and pressure angle) [13]. Zouari et al. [14, 15] adopted a 3D finite element method (FEM) to study the effects of propagation depth, orientation, and position in the blending radius of cracks on instantaneous mesh stiffness. 2D FEM was used to analyse the variation in stress intensity factor on the tooth base according to crack depth, crack propagation angle, and crack position. The propagation process was divided into two or four stages in [6, 7, 16, 17] to study the effect of severity of crack faults on mesh stiffness. In summary, crack length is assumed to be time-invariant in all these studies. As a result, the dynamic process of crack propagation has not been revealed.

In fact, according to the principle of fracture mechanics [18–20], crack arrest is a common phenomenon that occurs during crack propagation, given that cracks will propagate only if the crack driving force is greater than the crack resistance. During crack propagation, the crack driving force initially increases with the increase in crack length and then decreases. Crack arrest occurs when the driving force is lower than the resistance. For ductile materials, such as metal or alloy, when the initial crack propagates, a slow propagation stage occurs before rapid propagation. However, automatic crack arrest may appear in both slow and rapid propagation stages. The stress of the gear teeth changes rapidly for fast engaging-in and engaging-out of the gear teeth. This change may also result in the propagation and arrest of cracks in a short time, and the cracks rapidly propagate in tiny lengths.

Detection of crack propagation with a tiny length in a very short time (described above) is important in condition monitoring and fault diagnosis of a device. Thus, timely detection and confirmation of further propagation of cracks are highly necessary. Crack propagation by a tiny length in a short time is defined as transient propagation of cracks (TPOC). One of the contributions of this study is the investigation of TPOC for the timely detection and confirmation of further crack propagation. Only a few studies have investigated this aspect. Moreover, in this study, crack length is assumed to be time-varying to describe TPOC. Different TPOC models are proposed to simulate crack propagation instantaneously.

For the algorithm of time-varying mesh stiffness, two methods of calculating the time-varying mesh stiffness of a gear set exist [21]; these two methods are FEM and the analytical method (AM). The former is time-consuming because every gear pair must be modelled to determine the mesh stiffness of a range of gear pairs. Meanwhile, AM provides a general approach to evaluate mesh stiffness with satisfactory results [1]. The elastic deformation method has been introduced previously and has been used in other related studies [1, 22–24]. The potential energy method, a typical analytical method initially proposed by Yang and Lin, has been used to calculate the mesh stiffness of a pair of external-external spur gears [25]. Given its simple calculation process, the potential energy method has been adopted by a large number of scholars [3, 5–7, 17, 21, 26–28]. In this method, the gear tooth is usually modelled as a cantilever beam that begins at the base circle. The Hertzian energy, bending energy, and axial compressive energy corresponding to Hertzian contact stiffness, bending stiffness, and axial compressive stiffness are considered in this model. Eventually, the shear energy corresponding to shear stiffness was also considered in [26]. The potential energy method has been utilised to calculate the mesh stiffness of ring and cracked gears [27, 28], and both the mesh stiffness of a spur gear tooth with spatial crack propagation and a helical gear have been calculated with modified potential energy methods [29–31]. However, these studies regarded crack length as a constant when calculating mesh stiffness. Therefore, when a gear undergoes TPOC, the time-varying mesh stiffness cannot be calculated by existing algorithms. Although a series of different crack lengths have been used to represent crack propagation, at least two defects still exist. One is that the calculation is time-consuming because of multiple times of calculations, and the other is that only a series of discrete stiffness values for certain crack lengths can be obtained. Consequently, further propagation of cracks cannot be revealed by time-varying mesh stiffness. Instead of a constant, a propagation function is used to represent crack length in our improved potential energy method. With the improved method, the time-varying mesh stiffness when TPOC arises can be calculated, and further propagation of cracks can be detected in a timely manner.

In this study, TPOC was described and defined. Different propagation models were considered and proposed to simulate TPOC. The improved potential energy method was developed by incorporating the crack propagation model into the potential energy method. Four different deterioration levels of cracked gears were assumed, which means the lengths of existing cracks before TPOC were different. The crack was assumed to further propagate by a tiny length, as represented by the propagation model in each deterioration level. Afterwards, the time-varying mesh stiffness of gears when TPOC occurred was calculated with the improved method. The mesh stiffness variations caused by different TPOCs were compared and summarised.

2. The Transient Propagation of Crack and Improved Potential Energy Method

Crack propagation is a gradual process in which crack length increases. If crack length is assumed to be time-invariant, the dynamic process of crack propagation cannot be revealed. If the crack length of a cracked gear is considered constant, time-varying mesh stiffness cannot be calculated when the crack propagates by a tiny length in a very short time. Thus, crack propagation cannot be identified in a timely manner. Crack length has always been regarded as a constant when the potential energy method is adopted to calculate the time-varying mesh stiffness of gears [1, 3, 5–7, 17, 18, 24, 25]. In other words, the existing potential energy method cannot be directly used to calculate time-varying mesh stiffness when TPOC occurs in a gear. Before presenting our improved potential energy method, we introduce and describe TPOC. In this paper, TPOC is defined as the situation wherein cracks further propagate by a tiny length in a very short amount of time.

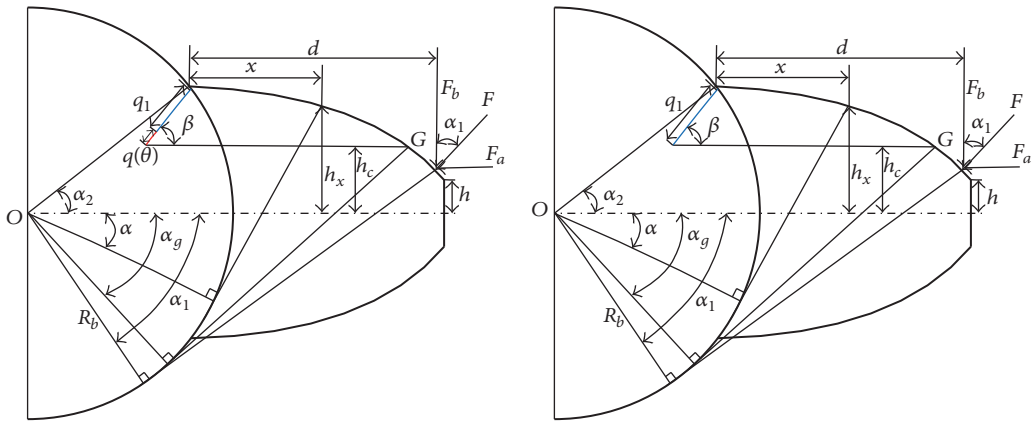

(a) TPOC appears (b) No TPOC

Figure 1: Nonuniform cantilever beam model of cracked gear.

2.1. Transient Propagation of Crack in a Pinion (Driving Gear)

2.1.1. Description of TPOC. We assume that TPOC appears in a pinion (driving gear). A crack exists before TPOC, and the length of the existing crack is q_1. The crack is assumed to propagate along a straight line and through the entire tooth width. The intersection angle, β, between the crack and the central line of the tooth is set at 45°. θ is the angle displacement of pinion (driving gear); the length of TPOC is represented by $q(\theta)$, where θ is time-varying; therefore, $q(\theta)$ is time-varying. The unit of $q(\theta)$ and θ is mm and rad, respectively. In Figure 1(a), the blue line is the existing crack, and the red line is TPOC. When the crack further propagates by a length of $q(\theta)$, the total length of the crack is $q_1 + q(\theta)$. If $q(\theta) = 0$, then the crack has not propagated and the crack length is constant, as shown in Figure 1(b).

2.1.2. Modelling of TPOC. Several transient propagation functions were modelled to describe TPOC. The function is shown with $q(\theta)$. The step function was used to represent the crack propagating by a tiny length instantaneously. A continuous step function was used to represent the crack propagating by several segments of tiny length instantaneously. A linear function was used to represent the crack propagating by a tiny length continuously in a very short time.

In the following functions, $q_{1a}(\theta)$ to $q_{1d}(\theta)$ are step functions. $q_2(\theta)$ is a continuous step function. $q_3(\theta)$ is a linear function. Therefore, the propagation model of $q_{1a}(\theta)$ to $q_{1d}(\theta)$ can be adopted to investigate the effects of different propagation lengths with the same propagation model on the time-varying mesh stiffness. Moreover, the propagation model of $q_2(\theta)$ and $q_3(\theta)$ can be adopted to study the effects of different propagation models with the same length on the time-varying mesh stiffness. All propagation models are expressed as follows.

(1) Different Propagation Lengths with the Same Propagation Model. As is shown in Figure 2(a),

$$q_{1a}(\theta) = \begin{cases} 0, & \theta < 0.02\text{rad} \\ 0.05, & \theta > 0.02\text{rad}, \end{cases}$$

$$q_{1b}(\theta) = \begin{cases} 0, & \theta < 0.02\text{rad} \\ 0.1, & \theta > 0.02\text{rad}, \end{cases}$$

$$q_{1c}(\theta) = \begin{cases} 0, & \theta < 0.02\text{rad} \\ 0.15, & \theta > 0.02\text{rad}, \end{cases}$$

$$q_{1d}(\theta) = \begin{cases} 0, & \theta < 0.02\text{rad} \\ 0.2, & \theta > 0.02\text{rad}. \end{cases} \tag{1}$$

(2) Different Propagation Models with the Same Propagation Length. As is shown in Figure 2(b), the purple line is $q_2(\theta)$, the red line is $q_3(\theta)$, and the total lengths of TPOCs are the same, that is, 0.15 mm, but their propagation modes are different from each other, which can be expressed as,

$$q_2(\theta) = \begin{cases} 0, & \theta < 0.02\text{rad} \\ 0.05, & 0.02\text{rad} < \theta < 0.04\text{rad} \\ 0.1, & 0.04\text{rad} < \theta < 0.06\text{rad} \\ 0.15, & \theta > 0.06\text{rad}, \end{cases} \tag{2}$$

$$q_3(\theta) = \begin{cases} 0, & \theta < 0.02\text{rad} \\ 3.75\theta - 0.075, & 0.02\text{rad} < \theta < 0.06\text{rad} \\ 0.15, & \theta > 0.06\text{rad}. \end{cases}$$

All the transient propagation models can be plotted in Figure 4.

2.2. Improved Algorithm of Mesh Stiffness When TPOC Occurs in a Pinion.

According to the potential energy method, the tooth can be regarded as a nonuniform cantilever beam shown in Figure 1(b). d represents the distance between the contact point and the root of the tooth, and the corresponding

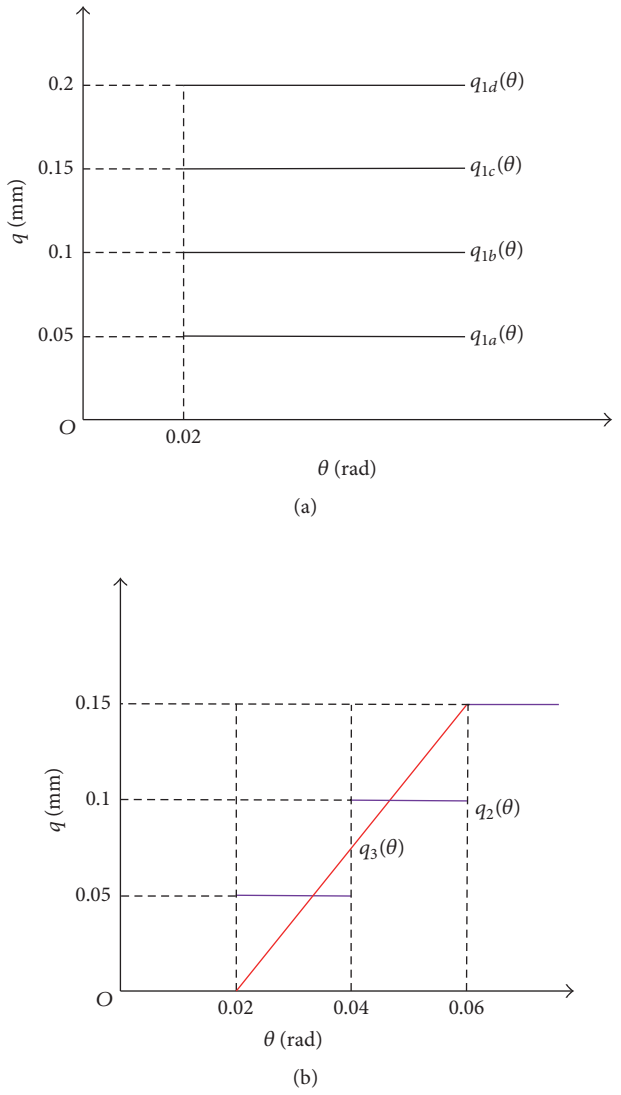

FIGURE 2: TPOC models. (a) Different propagation lengths with the same propagation model. (b) Different propagation models with the same propagation length.

angle is α_1. h_c represents the vertical distance between the tip of the crack and the tooth's central line, which corresponds to the angle α_g. R_b is the radius of base circle. α_2 is the half tooth angle on the base circle. q_1 is the length of existing crack. h is half of the roof chordal tooth thickness. β is the intersection angle between the crack and the central line of the tooth. The total potential energy stored in the gear system includes the following parts: the Hertzian contact energy, the bending energy, the axial compression energy, and the shear energy, which can be expressed as [7]

$$\begin{aligned} U_b &= \frac{F^2}{2k_b} = \int_0^d \frac{M^2}{2EI_x}dx, \\ U_a &= \frac{F^2}{2k_a} = \int_0^d \frac{F_a^2}{2EI_x}dx, \\ U_s &= \frac{F^2}{2k_s} = \int_0^d \frac{1.2F_b^2}{2GA_x}dx, \end{aligned} \tag{3}$$

where k_b, k_a, and k_s represent the bending stiffness, the axial compression stiffness, and the shear stiffness. E is Young's modulus. G is the shear modulus. Hence,

$$\begin{aligned} F_b &= F\cos\alpha_1, \\ F_a &= F\sin\alpha_1, \\ M &= F_a h, \end{aligned} \tag{4}$$

where F_a and F_b are the two perpendicular component forces of F and the torque M represents the bending effect of F_a.

I_x represents the area moment of inertia of the section where the distance from the tooth root is x; A_x represents the area of the section where the distance from the tooth root is x.

For a perfect gear without crack, I_x and A_x can be obtained as

$$\begin{aligned} I_x &= \frac{1}{12}(2h_x)^3 L, \\ A_x &= 2h_x L, \end{aligned} \tag{5}$$

where h_x is the distance between the point on the tooth's curve and the tooth's central line where the horizontal distance from the tooth root is x and L is the width of the tooth.

In this case, the bending stiffness, the axial compression stiffness, and the shear stiffness can be calculated by the following [7]:

$$\frac{1}{k_b} = \int_{-\alpha_1}^{\alpha_2} \frac{3\left[1+(\alpha_2-\alpha)\sin\alpha\cos\alpha_1-\cos\alpha\cos\alpha_1\right]^2(\alpha_2-\alpha)\cos\alpha}{2EL\left[(\alpha_2-\alpha)\cos\alpha+\sin\alpha\right]^3}d\alpha, \tag{6}$$

$$\frac{1}{k_s} = \int_{-\alpha_1}^{\alpha_2} \frac{1.2(1+\nu)(\alpha_2-\alpha)\cos\alpha\cos^2\alpha_1}{EL\left[(\alpha_2-\alpha)\cos\alpha+\sin\alpha\right]}d\alpha, \tag{7}$$

$$\frac{1}{k_a} = \int_{-\alpha_1}^{\alpha_2} \frac{(\alpha_2-\alpha)\cos\alpha\sin^2\alpha_1}{2EL\left[(\alpha_2-\alpha)\cos\alpha+\sin\alpha\right]}d\alpha. \tag{8}$$

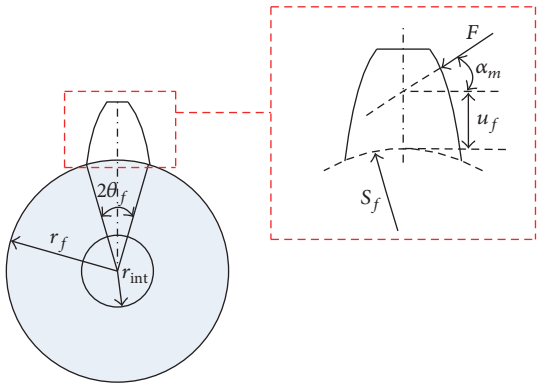

Figure 3: Geometrical parameters for the fillet-foundation deflection [28].

The fillet-foundation deflection was derived by Sainsot et al. in [32] based on the theory of [33]. It can be calculated as

$$\delta_f = \frac{F\cos^2\alpha_m}{LE} \times \left\{ N\left(\frac{u_f}{S_f}\right)^2 + M\left(\frac{u_f}{S_f}\right) + P\left(1 + Q\tan^2\alpha_m\right)\right\}, \tag{9}$$

where L represents the tooth width. u_f and S_f are given in Figure 2. The coefficients N, M, and P can be approached by polynomial functions [32]:

$$X_i\left(h_{fi}, \theta_f\right) = \frac{A_i}{\theta_f^2} + B_i h_{fi}^2 + \frac{C_i h_{fi}}{\theta_f} + \frac{D_i}{\theta_f} + E_i h_{fi} + F_i, \tag{10}$$

where X_i, denotes the coefficients N, M, P, and Q, $h_{fi} = r_f/r_{\text{int}}$, r_f and r_{int} are given in Figure 3, and the values of A_i, B_i, C_i, D_i, E_i, and F_i are given in Table 1.

The stiffness with consideration of gear fillet-foundation deflection can be obtained by

$$\frac{1}{k_f} = \frac{\delta_f}{F}. \tag{11}$$

For a cracked gear shown in Figure 1, I_x and A_x can be obtained as

$$I_x = \begin{cases} \frac{1}{12}\left(h_x + h_c\right)^3 L, & x \le g_c \\ \frac{1}{12}\left(2h_x\right)^3 L, & x > g_c, \end{cases} \qquad A_x = \begin{cases} \left(h_x + h_c\right) L, & x \le g_c \\ 2h_x L, & x > g_c. \end{cases} \tag{12}$$

In this study, the crack further propagates by a tiny length $q(\theta)$ instantaneously based on the existing crack, as shown in Figure 1(a). Therefore, the total crack length becomes $q_1 + q(\theta)$; then,

$$h_c = R_{b1}\sin\alpha_2 - \left[q_1 + q\left(\theta\right)\right]\sin\beta. \tag{13}$$

The crack only affects the bending stiffness and shear stiffness [17]; in this case, they change as follows:

$$\frac{1}{k_{cb}} = \int_{-\alpha_g}^{\alpha_2} \frac{12\left[1 + \left(\alpha_2 - \alpha\right)\sin\alpha\cos\alpha_1 - \cos\alpha\cos\alpha_1\right]^2\left(\alpha_2 - \alpha\right)\cos\alpha}{EL\left[\sin\alpha_2 + \sin\alpha + \left(\alpha_2 - \alpha\right)\cos\alpha - \left(\left(q_1 + q\left(\theta\right)\right)/R_b\right)\sin\beta\right]^3} d\alpha + \int_{-\alpha_1}^{-\alpha_g} \frac{3\left[1 + \left(\alpha_2 - \alpha\right)\sin\alpha\cos\alpha_1 - \cos\alpha\cos\alpha_1\right]^2\left(\alpha_2 - \alpha\right)\cos\alpha}{2EL\left[\left(\alpha_2 - \alpha\right)\cos\alpha + \sin\alpha\right]^3} d\alpha, \tag{14}$$

$$\frac{1}{k_{cs}} = \int_{-\alpha_g}^{\alpha_2} \frac{2.4\left(1 + \nu\right)\left(\alpha_2 - \alpha\right)\cos\alpha\cos^2\alpha_1}{EW\left[\sin\alpha_2 + \sin\alpha + \left(\alpha_2 - \alpha\right)\cos\alpha - \left(\left(q_1 + q\left(\theta\right)\right)/R_b\right)\sin\beta\right]} d\alpha + \int_{-\alpha_1}^{-\alpha_g} \frac{1.2\left(1 + \nu\right)\left(\alpha_2 - \alpha\right)\cos\alpha\cos^2\alpha_1}{EW\left[\left(\alpha_2 - \alpha\right)\cos\alpha + \sin\alpha\right]} d\alpha. \tag{15}$$

The time-varying mesh stiffness of the double-tooth pair can be calculated with (6) [23]. Hence,

$$k\left(\theta\right) = \sum_{i=1}^{2} \frac{1}{1/k_h + 1/k_{bc1,i} + 1/k_{sc1,i} + 1/k_{a1,i} + 1/k_{f1,i} + 1/k_{b2,i} + 1/k_{s2,i} + 1/k_{a2,i} + 1/k_{f2,i}}. \tag{16}$$

Table 1: Values of the coefficients of (10) [4].

	A_i	B_i	C_i	D_i	E_i	F_i
N	$-5.574E-5$	$-1.9986E-3$	$-2.3015E-4$	$4.7702E-3$	0.0271	6.8045
M	$60.111E-5$	$28.1E-3$	$-83.431E-4$	$-9.9256E-3$	0.1624	0.9086
P	$-50.952E-5$	$185.5E-3$	$0.0538E-4$	$53.3E-3$	0.2895	0.9236
Q	$-6.2042E-5$	$9.0889E-3$	$-4.0964E-4$	$7.8297E-3$	-0.1472	0.6904

Table 2: h_c before and after TPOC arises.

	No TPOC	TPOC arises
Case 1 Case 2	$h_c = R_{b1}\sin\alpha_2 - q_1\sin\beta$	$h_c = R_{b1}\sin\alpha_2 - [q_1 + q(\theta)]\sin\beta$
Case 3 Case 4	$h_c = q_2\sin\beta$	$h_c = [q_2 + q(\theta)]\sin\beta$

The subscripts 1 and 2 represent the pinion (driving gear) and gear (driven gear), respectively. $i = 1$ represents the first pair of meshing teeth when two pairs of teeth mesh; $i = 2$ represents the second pair. θ is the angle displacement of pinion (driving gear).

In (13), (14), and (15), q_1 is the length of existing length and $q(\theta)$ is the length of TPOC. The time-varying mesh stiffness when TPOC arises in a pinion (driving gear) can be solved with (8), (11), (14), (15), and (16).

3. Simulation Results and Discussion

Different deterioration levels of existing cracks were considered to study the influences of TPOC on time-varying mesh stiffness. In each deterioration level, TPOCs with the same model but different lengths and with the same length but different models were considered, and the resultant stiffness variations were compared.

3.1. Different Deterioration Levels of Crack before TPOC. Different lengths of existing cracks were considered, as shown in Figure 4. In Figure 4, cases 1 to 4 represent the length of the existing crack becoming increasingly large; that is, the deterioration level of the crack becomes increasingly serious. The blue line represents the existing crack; the red line represents TPOC. In cases 1 and 2, the length of the existing crack is q_1. In cases 3 and 4, the length of the existing crack is q_1+q_2. h_c before and after TPOC arises in the different cases as shown in Table 2.

According to the formula in Table 2, the bending and shear stiffness when TPOC arises can be recalculated as follows:

Case 1

$$\begin{aligned}\frac{1}{k_{cb}} &= \int_{-\alpha_g}^{\alpha_2} \frac{12\left[1+(\alpha_2-\alpha)\sin\alpha\cos\alpha_1-\cos\alpha\cos\alpha_1\right]^2(\alpha_2-\alpha)\cos\alpha}{EL\left[\sin\alpha_2+\sin\alpha+(\alpha_2-\alpha)\cos\alpha-\left((q_1+q(\theta))/R_b\right)\sin\beta\right]^3}d\alpha \\ &\quad+\int_{-\alpha_1}^{-\alpha_g}\frac{3\left[1+(\alpha_2-\alpha)\sin\alpha\cos\alpha_1-\cos\alpha\cos\alpha_1\right]^2(\alpha_2-\alpha)\cos\alpha}{2EL\left[(\alpha_2-\alpha)\cos\alpha+\sin\alpha\right]^3}d\alpha, \\ \frac{1}{k_{cs}} &= \int_{-\alpha_g}^{\alpha_2}\frac{2.4(1+\nu)(\alpha_2-\alpha)\cos\alpha\cos^2\alpha_1}{EW\left[\sin\alpha_2+\sin\alpha+(\alpha_2-\alpha)\cos\alpha-\left((q_1+q(\theta))/R_b\right)\sin\beta\right]}d\alpha \\ &\quad+\int_{-\alpha_1}^{-\alpha_g}\frac{1.2(1+\nu)(\alpha_2-\alpha)\cos\alpha\cos^2\alpha_1}{EW\left[(\alpha_2-\alpha)\cos\alpha+\sin\alpha\right]}d\alpha.\end{aligned} \tag{17}$$

Case 2

$$\begin{aligned}\frac{1}{k_{cb}} &= \int_{-\alpha_1}^{\alpha_2}\frac{12\left[1+(\alpha_2-\alpha)\sin\alpha\cos\alpha_1-\cos\alpha\cos\alpha_1\right]^2(\alpha_2-\alpha)\cos\alpha}{EW\left[\sin\alpha_2+\sin\alpha+(\alpha_2-\alpha)\cos\alpha-\left((q_1+q(\theta))/R_b\right)\sin\beta\right]^3}d\alpha, \\ \frac{1}{k_{cs}} &= \int_{-\alpha_1}^{\alpha_2}\frac{2.4(1+\nu)(\alpha_2-\alpha)\cos\alpha\cos^2\alpha_1}{EW\left[\sin\alpha_2+\sin\alpha+(\alpha_2-\alpha)\cos\alpha-\left((q_1+q(\theta))/R_b\right)\sin\beta\right]}d\alpha.\end{aligned} \tag{18}$$

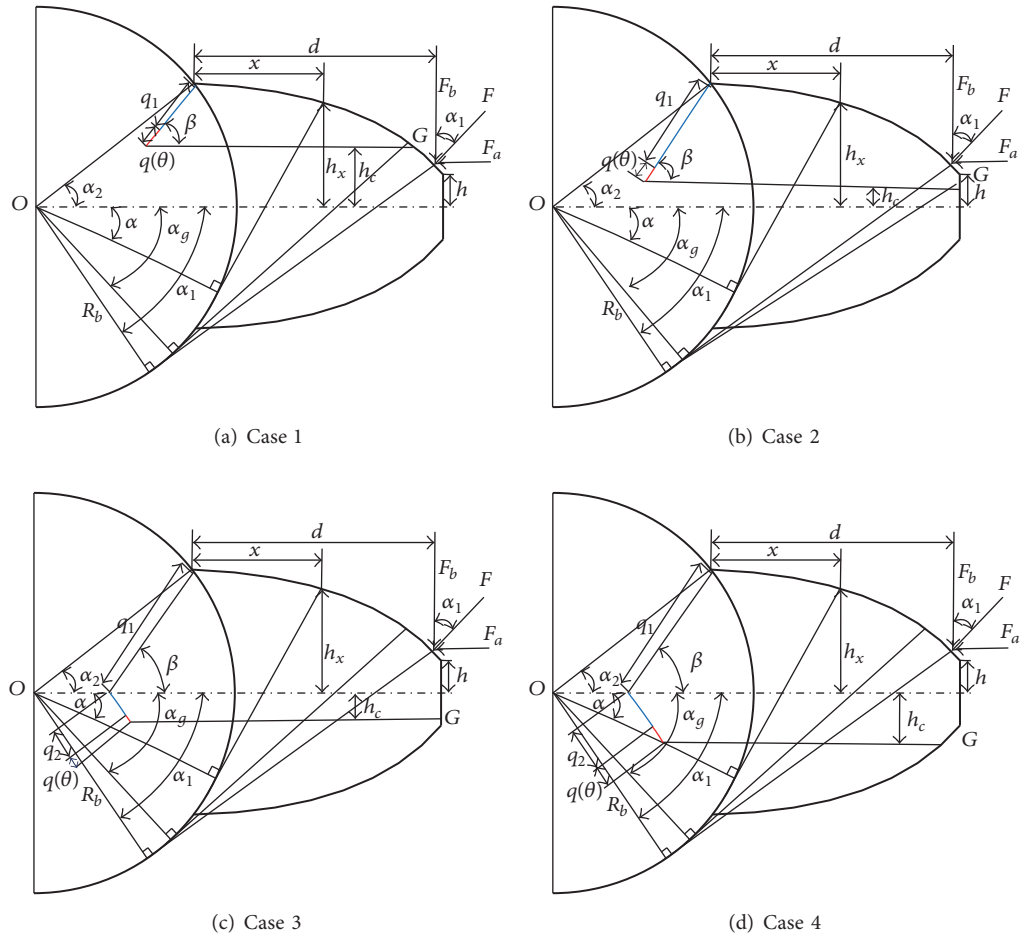

(a) Case 1 (b) Case 2

(c) Case 3 (d) Case 4

Figure 4: Different deterioration levels before TPOC.

Case 3

$$\frac{1}{k_{cb}} = \int_{-\alpha_1}^{\alpha_2} \frac{12\left[1+(\alpha_2-\alpha)\sin\alpha\cos\alpha_1-\cos\alpha\cos\alpha_1\right]^2(\alpha_2-\alpha)\cos\alpha}{EW\left[\sin\alpha+(\alpha_2-\alpha)\cos\alpha-\left((q_2+q(\theta))/R_b\right)\sin\beta\right]^3}d\alpha,$$

$$\frac{1}{k_{cs}} = \int_{-\alpha_1}^{\alpha_2} \frac{2.4(1+\nu)(\alpha_2-\alpha)\cos\alpha\cos^2\alpha_1}{EW\left[\sin\alpha+(\alpha_2-\alpha)\cos\alpha-\left((q_2+q(\theta))/R_b\right)\sin\beta\right]}d\alpha. \quad (19)$$

Case 4

$$\frac{1}{k_{cb}} = \int_{-\alpha_g}^{\alpha_2} \frac{12\left[1+(\alpha_2-\alpha)\sin\alpha\cos\alpha_1-\cos\alpha\cos\alpha_1\right]^2(\alpha_2-\alpha)\cos\alpha}{EW\left[\sin\alpha+(\alpha_2-\alpha)\cos\alpha-\left((q_2+q(\theta))/R_b\right)\sin\beta\right]^3}d\alpha,$$

$$\frac{1}{k_{cs}} = \int_{-\alpha_g}^{\alpha_2} \frac{2.4(1+\nu)(\alpha_2-\alpha)\cos\alpha\cos^2\alpha_1}{EW\left[\sin\alpha+(\alpha_2-\alpha)\cos\alpha-\left((q_2+q(\theta))/R_b\right)\sin\beta\right]}d\alpha. \quad (20)$$

Table 3: Main parameters of the gear system.

Gear type	Standard involute spur teeth
Material	Steel
Young's modulus	$E = 2.068 \times 10^{11}$ Pa
Poisson ratio	$\nu = 0.3$
Number of teeth	$N_1 = 19$ and $N_2 = 48$
Pressure angle	$\alpha = 20^\circ$
Diametral pitch	$P = 8$ inch^{-1}
Base radius of the gear	$R_{b1} = 28.34$ mm
Width of teeth	$w = 18$ mm
Mass of the pinion	$m_1 = 0.96$ Kg
Mass of the gear	$m_2 = 2.88$ Kg
Contact ratio	$C_r = 1.6456$
Mass moment of inertia of the motor	$I_m = 0.0021$ Kg m^2
Mass moment of inertia of the load	$I_b = 0.0105$ Kg m^2
Mass moment of inertia of the pinion	$I_1 = 4.3659 \times 10^{-4}$ Kg m^2
Mass moment of inertia of the gear	$I_2 = 8.3602 \times 10^{-3}$ Kg m^2

As a sample of the length of existing crack, q_1 (or q_1 and q_2) can be set in the following 4 cases. Case 1 to case 4 represent the notion that the deterioration level becomes more serious:

Case 1: when $q_1 = 1.57$

Case 2: when $q_1 = 3.13$

Case 3: when $q_1 = 3.92$ and $q_2 = 0.78$

Case 4: when $q_1 = 3.92$ and $q_2 = 2.35$

3.2. Time-Varying Mesh Stiffness Simulation When TPOC Occurs. Based on the improved potential energy method, the time-varying mesh stiffness when TPOC occurs in a pinion was calculated. The main parameters are shown in Table 3.

3.2.1. Mesh Stiffness Simulation When TPOC Occurs with the Same Model but Different Lengths. This section focuses on mesh stiffness when TPOC occurs with the model of a step function. However, the lengths are 0.05, 0.1, 0.15, and 0.2 mm. In Figure 5, $q(\theta) = 0$ indicates that no TPOC occurs, and the corresponding stiffness represents the mesh stiffness of a cracked gear with the length of an existing crack.

Figure 5 shows the time-varying mesh stiffness when TPOC occurs with different lengths under the same propagation model (i.e., step function model). Figure 5(a) depicts the mesh stiffness variation when $q_{1a}(\theta)$, $q_{1b}(\theta)$, $q_{1c}(\theta)$, and $q_{1d}(\theta)$ appear in case 1. Similarly, Figures 5(b), 5(c), and 5(d) depict the mesh stiffness variation when $q_{1a}(\theta)$, $q_{1b}(\theta)$, $q_{1c}(\theta)$, and $q_{1d}(\theta)$ appear in cases 2, 3, and 4, respectively.

Figure 5(a) shows that an instantaneous increment in the length of the crack induces a sudden decrease in mesh stiffness. Indeed, large lengths of crack propagation induce large reductions in mesh stiffness. The same phenomenon appears in the other cases. After TPOC, the total length of cracks is the sum of the existing crack length and TPOC length. Furthermore, the stiffness curve represents the time-varying mesh stiffness of gears with the total length of cracks.

The stiffness reduction caused by TPOC in different cases (compared with no TPOC when $q(\theta) = 0$) is listed in Table 4. In Table 4, $0.02^-/0.02^+$ represents the moment before/after TPOC arises and $k_{1i}(0.02^-)/k_{1i}(0.02^+)$ represents the mesh stiffness of the moment before/after TPOC occurs with the model of $q_{1i}(\theta)$ ($i = a, b, c, d$). A schematic of stiffness reduction is shown in Figure 7(a).

From Table 4 and Figure 7(a), we can see that, for the same length of TPOC with the model of step function, the resultant stiffness reduction becomes less gradually from case 1 to case 4. In other words, as the deterioration level of crack increases, the stiffness reduction caused by TPOC will decrease.

3.2.2. Mesh Stiffness Simulation for TPOC with the Same Length but Different Models. Similar to that in Figure 5, $q(\theta) = 0$ in Figure 6 indicates the absence of TPOC. The time-varying mesh stiffness when TCOP occurs with the same length but different propagation models is shown in Figure 6. In the figure, the crack instantaneously propagates by 0.015 mm in two different models: continuous step and linear function models. For TPOC with the linear function model, the length of TPOC changes continuously, and the resultant stiffness variation is also continuous and smooth. For the continuous step function model, several continuous mutations in propagation length lead to several sudden decrements in mesh stiffness. However, regardless of the TPOC model, the stiffness curve after TPOC overlaps; that is, the stiffness is equal after TPOC, when the transient propagation length remains constant.

We mainly investigated TPOC with the model of a continuous step function symbolized by $q_2(\theta)$. The transient propagation process is described with three segments of the step function, denoting that the crack has propagated the same small length for three incidents. The three segments of TPOC are represented with $q_{21}(\theta)$, $q_{22}(\theta)$ and $q_{23}(\theta)$, respectively.",

Table 5 shows the stiffness reduction caused by each segment of crack propagation of TPOC with the continuous step function model in different cases. In the table, $0.02^-/0.02^+$ represents the moment before/after TPOC from 0 mm to 0.05 mm, $0.04^-/0.04^+$ represents the moment before/after TPOC from 0.05 mm to 0.1 mm, and $0.06^-/0.06^+$ represents the moment before/after TPOC from 0.1 mm to 0.15 mm. $k_2(0.02^-)$, $k_2(0.02^+)$, $k_2(0.04^-)$, $k_2(0.04^+)$, $k_2(0.06^-)$, and $k_2(0.06^+)$ represent the mesh stiffness of the corresponding moment. A schematic of the stiffness reduction is shown in Figure 7(b).

Table 5 and Figure 7(b) show that, per 0.05 mm of TPOC, the resultant stiffness reduction decreases from case 1 to case 4. Therefore, we conclude that as the crack deterioration level becomes increasingly serious, the stiffness reduction caused by TPOC decreases.

4. Conclusions

Several TPOC models have been proposed to study the influences of TPOC on the time-varying mesh stiffness of the

Table 4: Mesh stiffness reduction caused by TPOC (with the model of step function but different lengths) in different deterioration levels.

Deterioration levels of crack before TP	TP model	Stiffness value (10^8 N/m)	Stiffness reduction caused by TPOC (10^8 N/m)
Case 1	$k_{1a}(0.02^-) = k_{1b}(0.02^-) = k_{1c}(0.02^-) = k_{1d}(0.02^-) = 6.831$		0
	$q_{1a}(\theta)$	$k_{1a}(0.02^+) = 6.791$	$\downarrow 0.04$
	$q_{1b}(\theta)$	$k_{1b}(0.02^+) = 6.744$	$\downarrow 0.087$
	$q_{1c}(\theta)$	$k_{1c}(0.02^+) = 6.696$	$\downarrow 0.135$
	$q_{1d}(\theta)$	$k_{1d}(0.02^+) = 6.649$	$\downarrow 0.182$
Case 2	$k_{1a}(0.02^-) = k_{1b}(0.02^-) = k_{1c}(0.02^-) = k_{1d}(0.02^-) = 5.681$		0
	$q_{1a}(\theta)$	$k_{1a}(0.02^+) = 5.645$	$\downarrow 0.036$
	$q_{1b}(\theta)$	$k_{1b}(0.02^+) = 5.598$	$\downarrow 0.083$
	$q_{1c}(\theta)$	$k_{1c}(0.02^+) = 5.551$	$\downarrow 0.13$
	$q_{1d}(\theta)$	$k_{1d}(0.02^+) = 5.503$	$\downarrow 0.178$
Case 3	$k_{1a}(0.02^-) = k_{1b}(0.02^-) = k_{1c}(0.02^-) = k_{1d}(0.02^-) = 3.461$		0
	$q_{1a}(\theta)$	$k_{1a}(0.02^+) = 3.43$	$\downarrow 0.031$
	$q_{1b}(\theta)$	$k_{1b}(0.02^+) = 3.383$	$\downarrow 0.078$
	$q_{1c}(\theta)$	$k_{1c}(0.02^+) = 3.337$	$\downarrow 0.124$
	$q_{1d}(\theta)$	$k_{1d}(0.02^+) = 3.293$	$\downarrow 0.168$
Case 4	$k_{1a}(0.02^-) = k_{1b}(0.02^-) = k_{1c}(0.02^-) = k_{1d}(0.02^-) = 2.68$		0
	$q_{1a}(\theta)$	$k_{1a}(0.02^+) = 2.654$	$\downarrow 0.026$
	$q_{1b}(\theta)$	$k_{1b}(0.02^+) = 2.607$	$\downarrow 0.073$
	$q_{1c}(\theta)$	$k_{1c}(0.02^+) = 2.561$	$\downarrow 0.119$
	$q_{1d}(\theta)$	$k_{1d}(0.02^+) = 2.516$	$\downarrow 0.164$

Table 5: Mesh stiffness reduction caused by TPOC with the model of a continuous step function in different deterioration levels.

Deterioration levels of crack before TP	TCP length (mm)	Stiffness value (10^8 N/m)	Reduction caused by TPOC (10^8 N/m)
Case 1	0.05	$k_2(0.02^-) = 6.831$ $k_2(0.02^+) = 6.791$	$\downarrow 0.04$
Case 1	0.1	$k_2(0.04^-) = 6.852$ $k_2(0.04^+) = 6.813$	$\downarrow 0.039$
Case 1	0.15	$k_2(0.06^-) = 6.812$ $k_2(0.06^+) = 6.781$	$\downarrow 0.031$
Case 2	0.05	$k_2(0.02^-) = 5.681$ $k_2(0.02^+) = 5.645$	$\downarrow 0.036$
Case 2	0.1	$k_2(0.04^-) = 5.706$ $k_2(0.04^+) = 5.673$	$\downarrow 0.033$
Case 2	0.15	$k_2(0.06^-) = 5.672$ $k_2(0.06^+) = 5.641$	$\downarrow 0.031$
Case 3	0.05	$k_2(0.02^-) = 3.461$ $k_2(0.02^+) = 3.43$	$\downarrow 0.031$
Case 3	0.1	$k_2(0.04^-) = 3.609$ $k_2(0.04^+) = 3.581$	$\downarrow 0.028$
Case 3	0.15	$k_2(0.06^-) = 3.789$ $k_2(0.06^+) = 3.763$	$\downarrow 0.026$
Case 4	0.05	$k_2(0.02^-) = 2.68$ $k_2(0.02^+) = 2.654$	$\downarrow 0.026$
Case 4	0.1	$k_2(0.04^-) = 2.833$ $k_2(0.04^+) = 2.808$	$\downarrow 0.025$
Case 4	0.15	$k_2(0.06^-) = 3.014$ $k_2(0.06^+) = 2.992$	$\downarrow 0.022$

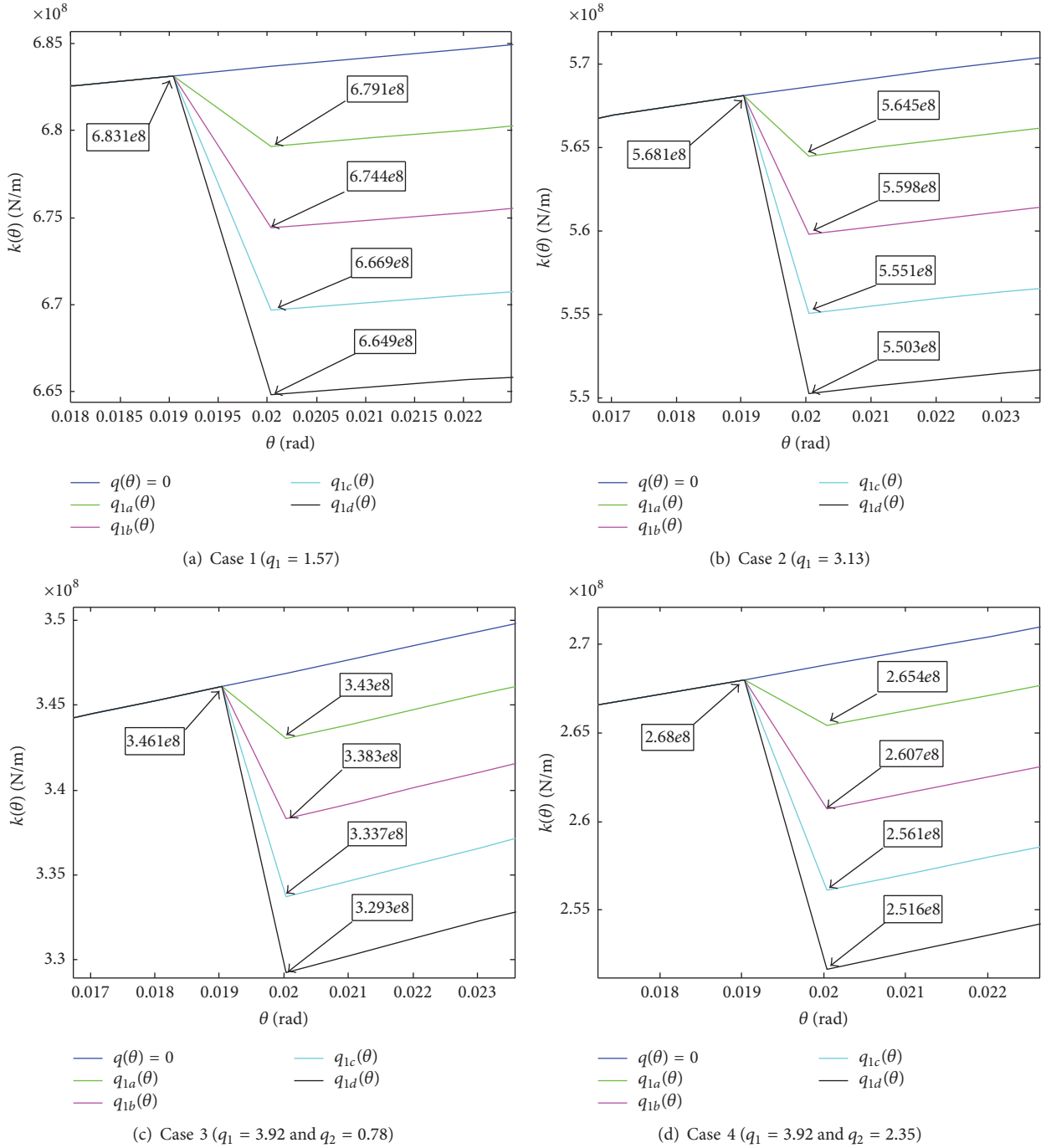

FIGURE 5: The influences of TPOC with different lengths but the same propagation model on mesh stiffness. $q_{1a}(\theta)$, $q_{1b}(\theta)$, $q_{1c}(\theta)$, and $q_{1d}(\theta)$ represent the crack propagating with the model of a step function, which indicates that the crack has instantaneously propagated by a tiny length. The corresponding lengths are 0.05, 0.1, 0.15, and 0.2 mm. $q(\theta) = 0$ represents the absence of TPOC.

gear and detect the further propagation of cracks from the perspective of time-varying mesh stiffness in a timely manner. The improved potential energy method was developed by integrating the TPOC model into the potential energy method. The simulation results show that the improved potential energy method can accurately calculate the time-varying mesh stiffness when TPOC occurs. Different deterioration levels of cracks before TPOC, different propagation models, and different lengths of TPOC were considered. The following conclusions were obtained:

(1) The stiffness variation trend is similar to that in the model of TPOC which caused the variation. For example, when TPOC occurs with the model of a step function, the resultant stiffness variation is in the form of an approximate step function. When TPOC occurs with the model of a continuous step function,

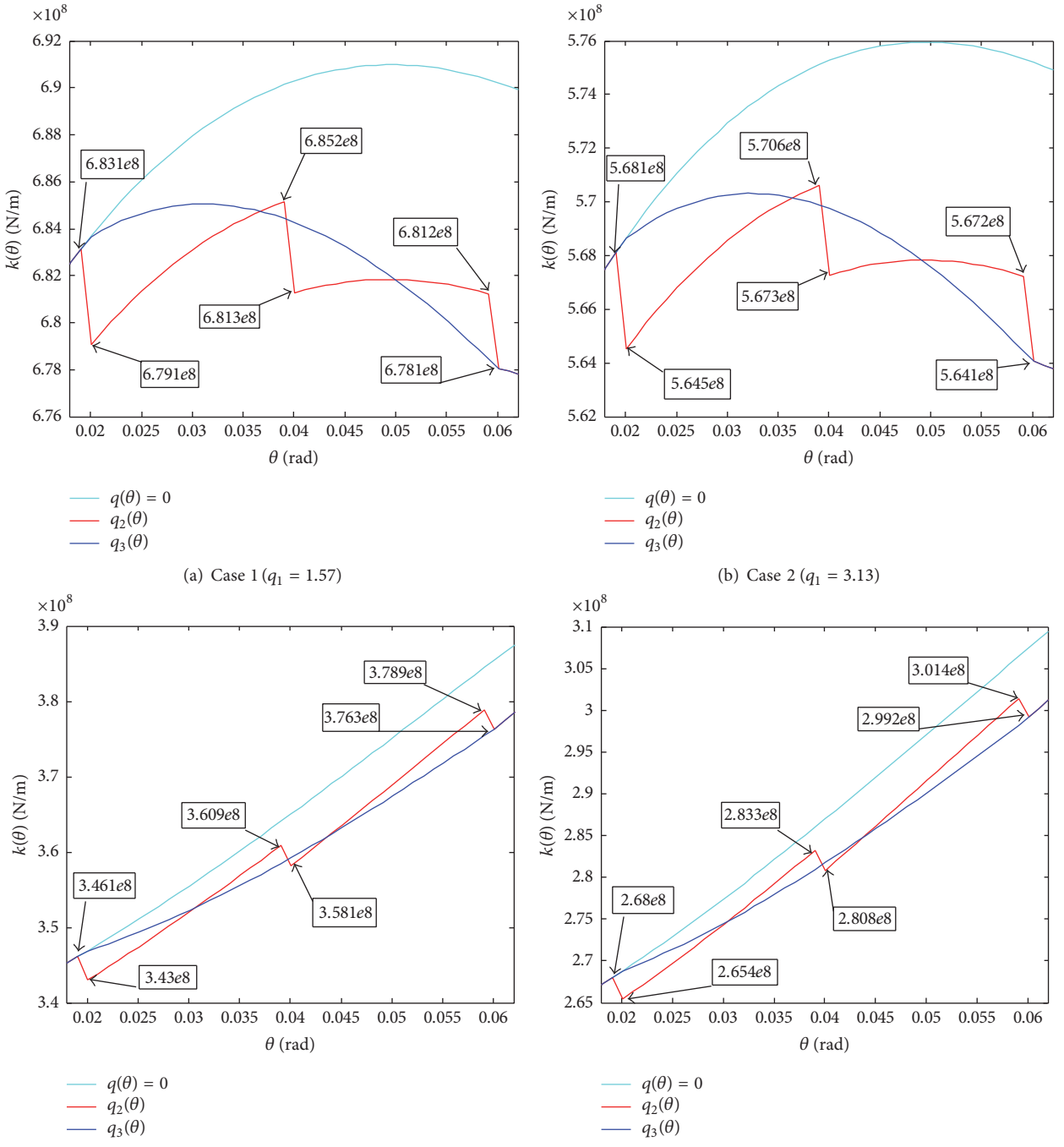

FIGURE 6: The influences of TPOC with the same length but different propagation models on mesh stiffness. $q_2(\theta)$ and $q_3(\theta)$ represent the crack propagating with the same length of 0.15 mm. $q_2(\theta)$ represents the crack with the model of a continuous step function, indicating that the crack has instantaneously propagated by several continuous segments of length. $q_3(\theta)$ represents the crack propagating with the model of a linear function, indicating that the crack has propagated continuously and smoothly. $q(\theta) = 0$ represents the absence of TPOC.

the resultant stiffness variation is in the form of an approximate continuous step function. When TPOC occurs with the model of a linear function, the resultant stiffness variation is smooth and continuous.

(2) For the certain deterioration level of cracks before transient propagation, large propagation lengths are associated with large variations in stiffness.

(3) When the crack propagates by the same tiny length instantaneously (e.g., TPOC occurs with the model of a step function), the resultant stiffness reduction decreases as the deterioration level of the crack increases (cases 1 to 4). When the crack continuously propagates by several segments of equal length (e.g., TPOC arises with the model of a continuous

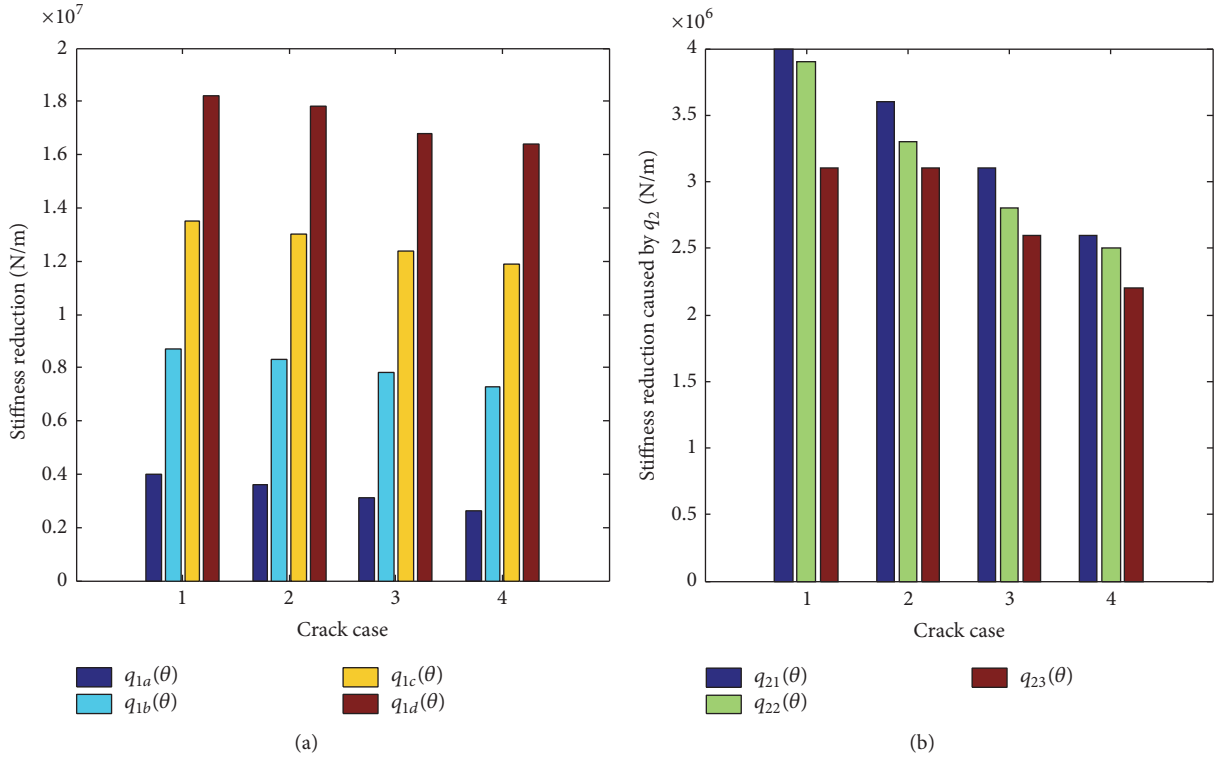

Figure 7: Mesh stiffness reduction caused by TCOP models in all cases.

step function), for every equal length of TPOC, the resultant stiffness reduction decreases gradually from case 1 to case 4. Therefore, we conclude that, for the same length of TPOC, the resultant stiffness reduction is related to the deterioration level of the crack; high levels of deterioration are associated with small reductions in stiffness. In other words, TPOC is easy to detect in the early stage of a gear fault.

(4) For a cracked gear, identical transient propagation lengths result in identical stiffness levels after TPOC regardless of the type of TPOC.

Competing Interests

The authors declare that they have no competing interests.

Acknowledgments

The work here is supported by the National Natural Science Foundation of China (no. 51175208, no. 51075161).

References

[1] F. Chaari, T. Fakhfakh, and M. Haddar, "Analytical modelling of spur gear tooth crack and influence on gearmesh stiffness," *European Journal of Mechanics—A/Solids*, vol. 28, no. 3, pp. 461–468, 2009.

[2] G. Litak and M. I. Friswell, "Dynamics of a gear system with faults in meshing stiffness," *Nonlinear Dynamics*, vol. 41, no. 4, pp. 415–421, 2005.

[3] Y. Shao and Z. Chen, "Dynamic features of planetary gear set with tooth plastic inclination deformation due to tooth root crack," *Nonlinear Dynamics*, vol. 74, no. 4, pp. 1253–1266, 2013.

[4] C. J. Li and H. Lee, "Gear fatigue crack prognosis using embedded model, gear dynamic model and fracture mechanics," *Mechanical Systems and Signal Processing*, vol. 19, no. 4, pp. 836–846, 2005.

[5] O. D. Mohammed, M. Rantatalo, and J.-O. Aidanpää, "Improving mesh stiffness calculation of cracked gears for the purpose of vibration-based fault analysis," *Engineering Failure Analysis*, vol. 34, pp. 235–251, 2013.

[6] X. H. Tian, *Dynamic simulation for system response of gearbox including localized gear faults [M.S. thesis]*, University of Alberta, 2004.

[7] S. Wu, *Gearbox dynamic simulation and estimation of fault growth [M.S. thesis]*, University of Alberta, 2007.

[8] D. G. Lewicki and R. Ballarini, "Effect of rim thickness on gear crack propagation path," *Journal of Mechanical Design*, vol. 119, no. 1, pp. 88–95, 1997.

[9] D. G. Lewicki and R. Ballarini, "Gear crack propagation investigations," *Gear Technology*, vol. 14, no. 6, pp. 18–24, 1997.

[10] D. G. Lewicki, L. E. Spievak, P. A. Wawrzynek, A. R. Ingraffea, and R. F. Handschuh, "Consideration of moving tooth load in gear crack propagation predictions," *Gear Technology*, vol. 19, no. 1, pp. 14–21, 2002.

[11] Y. Pandya and A. Parey, "Failure path based modified gear mesh stiffness for spur gear pair with tooth root crack," *Engineering Failure Analysis*, vol. 27, pp. 286–296, 2013.

[12] Y. Pandya and A. Parey, "Simulation of crack propagation in spur gear tooth for different gear parameter and its influence on

mesh stiffness," *Engineering Failure Analysis*, vol. 30, pp. 124–137, 2013.

[13] Y. Pandya and A. Parey, "Crack behavior in a high contact ratio spur gear tooth and its effect on mesh stiffness," *Engineering Failure Analysis*, vol. 34, pp. 69–78, 2013.

[14] S. Zouari, M. Maatar, T. Fakhfakh, and M. Haddar, "Three-dimensional analyses by finite element method of a spur gear: effect of cracks in the teeth foot on the mesh stiffness," *Journal of Failure Analysis and Prevention*, vol. 7, no. 6, pp. 475–481, 2007.

[15] S. Zouari, M. Maatar, T. Fakhfakh, and M. Haddar, "Following spur gear crack propagation in the tooth foot by finite element method," *Journal of Failure Analysis and Prevention*, vol. 10, no. 6, pp. 531–539, 2010.

[16] X. Tian, M. J. Zuo, and K. R. Fyfe, "Analysis of the vibration response of a gearbox with gear tooth faults," in *Proceedings of the ASME International Mechanical Engineering Congress and Exposition (IMECE04 '04)*, pp. 785–793, Anaheim, Calif, USA, November 2004.

[17] S. Wu, M. J. Zuo, and A. Parey, "Simulation of spur gear dynamics and estimation of fault growth," *Journal of Sound and Vibration*, vol. 317, no. 3–5, pp. 608–624, 2008.

[18] T. Fan, *Fracture Dynamics Principles and Applications*, Beijing Institute of Technology Press, 2006.

[19] G. R. Irwin and A. A. Wells, "A continuum-mechanics view of crack propagation," *Metallurgical Reviews*, vol. 10, no. 1, pp. 223–270, 1965.

[20] G. T. Hahn, R. G. Hoagland, M. F. Kanninen, and A. R. Rosenfield, "A preliminary study of fast fracture and arrest in the DCB test specimen," in *Proceedings of an International Conference on Dynamic Crack Propagation*, G. C. Sih, Ed., pp. 649–663, Springer, Berlin, Germany, 1973.

[21] X. Liang, M. J. Zuo, and T. H. Patel, "Evaluating the time-varying mesh stiffness of a planetary gear set using the potential energy method," *Proceedings of the Institution of Mechanical Engineers Part C: Journal of Mechanical Engineering Science*, vol. 228, no. 3, pp. 535–547, 2014.

[22] C. Weber, *The Deformation of Loaded Gears and the Effect on Their Load Carrying Capacity*, Report: British Department of Scientific and Industrial Research: Sponsored Research no. 3, 1949.

[23] Y. Attia, "Deflection of spur gear teeth cut in thin rims," *Journal of Engineering for Industry*, vol. 86, no. 4, pp. 333–341, 1963.

[24] R. W. Cornell, "Compliance and stress sensitivity of spur gear teeth," *Journal of Mechanical Design*, vol. 103, no. 2, pp. 447–459, 1981.

[25] D. C. H. Yang and J. Y. Lin, "Hertzian damping, tooth friction and bending elasticity in gear impact dynamics," *Journal of Mechanisms, Transmissions, and Automation in Design*, vol. 109, no. 2, pp. 189–196, 1987.

[26] X. Zhou, Y. Shao, Y. Lei, and M. Zuo, "Time-varying meshing stiffness calculation and vibration analysis for a 16DOF dynamic model with linear crack growth in a pinion," *Journal of Vibration and Acoustics*, vol. 134, no. 1, Article ID 011011, 2012.

[27] X. Liang, M. J. Zuo, and M. Pandey, "Analytically evaluating the influence of crack on the mesh stiffness of a planetary gear set," *Mechanism and Machine Theory*, vol. 76, pp. 20–38, 2014.

[28] Z. Chen and Y. Shao, "Dynamic simulation of planetary gear with tooth root crack in ring gear," *Engineering Failure Analysis*, vol. 31, pp. 8–18, 2013.

[29] W. Yu, Y. Shao, and C. K. Mechefske, "The effects of spur gear tooth spatial crack propagation on gear mesh stiffness," *Engineering Failure Analysis*, vol. 54, pp. 103–119, 2015.

[30] Z. Chen, W. Zhai, Y. Shao, K. Wang, and G. Sun, "Analytical model for mesh stiffness calculation of spur gear pair with non-uniformly distributed tooth root crack," *Engineering Failure Analysis*, vol. 66, pp. 502–514, 2016.

[31] Z. Wan, H. Cao, Y. Zi, W. He, and Y. Chen, "Mesh stiffness calculation using an accumulated integral potential energy method and dynamic analysis of helical gears," *Mechanism and Machine Theory*, vol. 92, pp. 447–463, 2015.

[32] P. Sainsot, P. Velex, and O. Duverger, "Contribution of gear body to tooth deflections—a new bidimensional analytical formula," *Journal of Mechanical Design*, vol. 126, no. 4, pp. 748–752, 2004.

[33] N. L. Muskhelishvili, *Some Basic Problems of the Mathematical Theory of Elasticity*, P. Noordhoff Limited, Amsterdam, The Netherlands, 2nd edition, 1975.